Shallow Normal Faulting and Block Rotation Associated with the 1975 Kalapana Earthquake, Kilauea Volcano, Hawaii[1,2]

Eric C. Cannon[3], Department of Geology, One Shields Avenue,
University of California, Davis, CA, 95616; phone: (530) 752-0350
e-mail: cannon@geology.ucdavis.edu

Roland Bürgmann, Department of Earth and Planetary Science, 307 McCone Hall,
University of California, Berkeley, Berkeley, CA 94720-4767; phone: (510) 643-9545
email: burgmann@seismo.berkeley.edu

Susan E. Owen, Science Hall, Room 125,
University of Southern California Earth Sciences,
Los Angeles, CA 90089-0740; phone: (213) 740-6308
email: owen@earth.usc.edu

(Submitted 05-16-00 to the *Bulletin of the Seismological Society of America*)
(Submitted 03-28-01 with revisions to the *Bulletin of the Seismological Society of America*)

[1] More information available at http://perry.geo.berkeley.edu/~burgmann/RESEARCH/research.html
[2] Digital supplemental materials available at ftp://quake.geo.berkeley.edu/outgoing/hawaii/BSSA_2000
[3] Present address: Department of Geological Sciences, University of Colorado at Boulder, Boulder, CO 80309-0399; phone: (303) 492-2763, fax: (303) 492-2606; e-mail: Eric.Cannon@Colorado.edu

Abstract

The Hilina fault system is a set of normal faults that accommodate extension of the mobile south flank of Kilauea Volcano. Large earthquakes (M≥6) and aseismic fault slip transport the flank southeastward along a basal detachment at ~8-10 km depth. Both the 1975 M7.2 Kalapana and the 1868 M7.9 Great Kau earthquakes produced slip on the Hilina faults. We compare Kalapana earthquake fault offsets, ground displacements derived from analysis of geodetic surveys, and model displacements from a dislocation model to evaluate whether the central Hilina fault slip associated with the Kalapana earthquake was due to a) shallow normal faulting independent of basal detachment slip or b) deep normal faulting directly linked to basal detachment slip. Our analysis shows that observed site motions at the coast are significantly greater than model displacements expected from a dislocation model of basal detachment slip alone. To explain ground displacements and fault offsets, we require fault slip on shallow normal faults (as deep as 2-3 km) triggered by slip on the basal detachment. Leveling data along the Chain of Craters Road and vertical fault offsets across the central Hilina fault system suggest that the Kalapana earthquake produced block rotation of the hanging wall blocks.

Introduction

Several major earthquakes (M≥6) have occurred on the south flank of Kilauea Volcano, Hawaii in historic times (~M7 1823, ~M7.9 1868, M6.5 1954, M7.2 1975, M6.1 1989). Hazards associated with major Kilauea earthquakes include significant ground subsidence and tsunamis (Tilling et al., 1976; Lipman et al., 1985, Ma et al., 1999). Major earthquakes could also trigger potentially catastrophic landslides (Moore et al., 1994; Moore and Chadwick, 1995). These earthquakes appear to involve slip along an ~8-10-km-deep, subhorizontal basal detachment, driven by rift intrusions and gravitational spreading (Swanson et al., 1974; Dieterich, 1988; Delaney and Denlinger, 1999). The M_l=7.2 November 29, 1975 Kalapana earthquake (hereinafter referred to as the Kalapana earthquake), the largest south flank earthquake in the twentieth century, generated a local tsunami 14 m high and produced up to 8 m of horizontal seaward displacement and 3.5 m of subsidence in coastal regions (Lipman et al., 1985). Similar coastal subsidence and tsunami were observed following the ~M7.9 1868 Great Kau earthquake (Swanson et al., 1974; Wyss, 1988). The Great Kau and Kalapana earthquakes both produced extensive surface rupture along the Hilina fault system (Lipman et al., 1985; Wyss, 1988; Bryan, 1992).

The relationship between slip on the Hilina fault system (Figure 1) and slip on the basal detachment is poorly understood. We study their interaction by comparing fault offset measurements along the central Hilina faults, ground displacements of coseismic deformation, and predicted displacements from a dislocation model representing basal detachment slip. We find that models of surface displacements due to basal slip alone significantly underestimate site motions of coastal geodetic stations along the central Hilina fault system. To better explain ground displacements

associated with the Kalapana earthquake, we present a revised kinematic model requiring slip on shallow Hilina normal faults in addition to slip on the deep basal detachment.

Tectonic Setting

Main shock focal mechanism studies of the Kalapana earthquake (Ando, 1979; Furumoto and Kovach, 1979) and ground displacements determined from geodetic measurements (Lipman et al., 1985; Delaney et al., 1998; Denlinger and Okubo, 1995) indicate southeast transport of the wedge-shaped south flank along an ~8-10-km-deep subhorizontal fault striking approximately northeast. Aftershocks were particularly active on a shallowly north-dipping band of microseismicity (Ando, 1979; Got et al., 1994; Gillard et al., 1996). This seismicity (Figure 2a) may identify a weak layer of ocean sediment that separates the mobile south flank block from the Cretaceous Pacific oceanic lithosphere (Hill, 1969; Nakamura, 1980; Thurber and Gripp, 1988). Multiplet relocation of earthquakes collapses a 2-3-km-thick zone of seismicity into a 100-200-m-thick band of seismicity at 8.5±1.5 km depth that dips 6°±-4° northward (Got et. al, 1994; Rubin et al., 1999). Bryan (1992) identified a similar concentration of aftershocks at 10 km depth for the M6.1 1989 earthquake. Kinematic inversions for the 1989 fault rupture plane based on leveling data coincide with the concentration of aftershocks (Árnadóttir et al., 1991).

Even though the majority of Kalapana earthquake coseismic moment release resulted from slip on the basal detachment, extensive normal faulting was documented on the surface along the Hilina fault system. Over 25 km of surface rupture occurred along the Hilina fault system from the Kalapana earthquake (Lipman et al., 1985). Lipman et al. (1985) suggested that ~1.5 m of vertical offset along much of the Hilina faults could account for approximately two-thirds of the coastal subsidence, implying

that the Hilina fault system played a significant role in south flank deformation associated with the Kalapana earthquake. Kellogg and Chadwick (1987) collected the first detailed fault offset measurements from the Kalapana earthquake (Figure 3). Fault morphology and offset of prehistoric volcanic units along the Hilina fault system suggest prior fault offset from major earthquakes (Tilling et al., 1976; Cannon and Bürgmann, 2001).

The Kalapana earthquake produced a marked change in the style of south flank deformation. From 1896 to the Kalapana earthquake, as much as 1 m northwest-southeast shortening occurred across the central south flank region (Swanson et al., 1974). After the Kalapana earthquake, geodetic baselines show contraction across the south flank until about 1981 and extension since then, except during time periods with rift intrusions (Delaney et al., 1998). Between 1983 and 1996, the south flank has been rapidly displacing to the southeast with little internal deformation (Delaney et al., 1998; Owen et al., 1995, Owen et al., 1999). The observed post-1982 displacement field can be modeled as aseismic slip on a 9-km-deep horizontal basal detachment with concurrent rift zone opening between 3 and 9 km depth (Delaney et al., 1993; Owen et al., 1995). Geodetic baselines across the Hilina faults have essentially remained unchanged since the Kalapana earthquake consistent with block-like seaward motion of the south flank (Delaney et al., 1998).

Kinematic Models of the South Flank

The Hilina faults display arcuate, south-facing, normal fault scarps trending east to northeast with a maximum scarp height of ~500 m. Two structural models exist for the Hilina faults, a "shallow" and "deep" model (Figure 2). An ~8-10-km-deep basal detachment and surface expression of the Hilina normal faults are common to both models. In the "deep" model (Figure 2b), the Hilina faults descend to the basal

detachment as normal fault splays. The "shallow" model (Figures 2c and 2d) treats slip on the Hilina fault system as independent of the basal detachment slip. Triggering mechanisms for slip on the Hilina faults may be different for both models. The "shallow" model could produce a greater risk of catastrophic landslides from slip on shallow slump structures than would be associated with the "deep" model of the Hilina fault system.

Several lines of evidence support a shallow fault interpretation. The arcuate surface traces of the Hilina faults resemble spoon-shaped listric normal faults commonly associated with slump structures. Riley et al. (1999) conducted a paleomagnetic study of the rotation of lava flows in the Puu Kapukapu block relative to lava flows exposed in the Hilina Pali fault scarp (Figure 1). In the western Hilina fault system, they propose that over the last 35.8 ky, the Puu Kapukapu block has experienced 12°±6° of landward rotation on a listric normal fault that extends to a depth of approximately 5 km. Ponding of lava flows against the fault scarps also suggests landward rotation of hanging wall blocks (Swanson et al., 1974). A hyaloclastic layer at 1-3 km depth (Moore and Fiske, 1969; Swanson et al., 1974) could act as a shallow basal detachment for Hilina faults. Morgan et al. (2000) identified seismic reflectors offshore of Halape (Figure 1) at the base of a 2-3-km-thick slump block composed of hyaloclastic material. These reflectors are interpreted as possible subsurface extensions of the Hilina fault system forming a detachment surface beneath the slump block.

The “deep” model presents the Hilina fault system as deeply-rooted normal faults splaying off the ~8-10-km-deep basal detachment (Lipman et al., 1985; Okubo et al., 1997). A concentration of microseismicity at 8-10 km depth beneath the upper south flank (Figure 2a) may indicate the intersection of the deep Hilina Pali fault with the basal detachment (Okubo et al., 1996). P-wave tomographic studies show a significant

lateral velocity gradient steeply dipping to the southeast beneath the Hilina fault system (Okubo et al, 1996). This velocity gradient, separating low velocity seaward rocks from high velocity inland rocks, may indicate the presence of the Hilina Pali normal fault descending to the basal detachment.

Measurements of Fault Offsets Associated with the Kalapana Earthquake

We analyze ground fractures and geodetic data associated with the Kalapana earthquake to improve our understanding of the fault geometry and kinematics of Kilauea's south flank. To document the Kalapana earthquake ground fractures, we measure the fault offset of sawtooth-shaped extension fractures in the 1969-1974 Mauna Ulu lava flows using several techniques from Jackson et al. (1992). We measure the plunge, azimuth, and magnitude of fault offsets preserved in Mauna Ulu pahoehoe lava flows that drape the central Hilina fault system. Fractures are not concentrated along a single fault strand but are distributed over a several 10's-of-meters-wide fracture zone. To measure fault offset across a fracture zone, we sum multiple individual fault offsets along traverses perpendicular to the general trend of the fault scarp. As an example, horizontal offset vector T50 in Figure 3a is calculated by summing 18 individual measurements of horizontal fault offset (labeled "a" through "r"). Seventy three fault offset traverses contain over 700 individual fault offset measurements (Figure 3; data presented in digital supplemental material Table DSM_1).

We summarize the trend of over 18,000 m of fracture (Digital supplemental material Table DSM_2) and over 200 fault offset measurements (Digital supplemental material Table DSM_ 3) on the Poliokeawe Pali, Holei Pali, and Apua Pali faults in Table 1. Fracture trends and fault offset azimuths are perpendicular to each other within uncertainties for all three faults indicating extension without a significant lateral shear component. Average fault offset azimuths trend generally southeast, parallel to

the south flank displacement associated with the Kalapana earthquake (Figure 1). The largest Kalapana earthquake fault offset for any Hilina fault is located on the Holei Pali where we measured 3.3 m of total offset summed along a traverse of 16 individual measurements.

We assume fractures in the Mauna Ulu lava flows are tectonic in origin resulting from fault slip along the Hilina fault system associated with the Kalapana earthquake. There is no evidence for compressional fold and fault structures at the base of the fault scarps, arguing against mass movement as the source of surface fractures. Where safe conditions exist, we descended into fractures to observe the fracture surface. There are no occurrences of slip surfaces parallel or sub-parallel to the bases of lava flows, suggesting that the upper few meters of Mauna Ulu pahoehoe lava had not simply detached from the subsurface to produce surface fractures. Even though fracture azimuth trends (Table 1) are generally perpendicular to the direction of south flank aseismic displacement and Kalapana earthquake displacement, fractures seem to trend parallel with local fault traces. These observations suggest that the local fault geometry influences the coseismic rupture pattern.

Comparison of Ground and Model Displacements with Fault Offsets

We propose that slip on both the shallow Hilina fault system and the ~8-10-km deep basal detachment slip contributed to coastal displacement associated with the Kalapana earthquake. Our initial kinematic model is schematically illustrated in Figure 4. The model consists of dislocations that approximate rift zone opening and slip along the basal detachment. No dislocation is included for the Hilina fault system. For a basal detachment slip event, this model predicts that geodetic stations landward or seaward of the Hilina fault system (i.e., on the footwall and hanging wall block of the Hilina fault system) will be displaced toward the southeast by similar amounts (open

vectors in Figure 4) relative to a fixed station northwest of the rift zone. If in addition to basal detachment slip, secondary slip occurs on the Hilina fault system, geodetic stations on the hanging wall of the Hilina fault system will experience increased motion due to basal detachment slip and slip on the Hilina normal faults. Residuals s1 and s2 (Figure 4) represent the difference between model and ground displacement, a value we suggest is attributed to slip on the Hilina fault system.

Horizontal ground displacements computed from trilateration data using a model coordinate solution (Matthews and Segall, 1993) and vertical ground displacements obtained from tide gage and leveling data (Figures 5a and 5b) are calculated relative to geodetic station HVO162 on the footwall of the central Hilina fault system. By calculating displacements relative to HVO162, we resolve the motions of the coastal geodetic stations located on the hanging wall of the Hilina fault system relative to the footwall block. We observe that the extension and elevation changes are greatest for coastal geodetic stations located on the hanging wall blocks. The Hilina footwall block itself moved significantly to the southeast with respect to stations north of Kilauea caldera and the rift zones, as noted by northwest-trending solid vectors of 1-3 m magnitude in Figure 5a.

To separate and evaluate the contributions of the Hilina fault system and basal detachment on the surface displacements, we calculate model displacements as a function of basal detachment slip only (open vectors in Figures 5c and 5d). We utilize model displacements calculated from a variable-slip dislocation model of the Kalapana earthquake derived from an inversion of available geodetic data (reanalysis of trilateration, leveling, and tilt data collected by Hawaiian Volcano Observatory, Lipman et al., 1985). For the inversion, we exclude geodetic data from geodetic stations (Figure 1) in the hanging wall of the Hilina faults to ensure model displacements are not biased

by non-basal detachment slip. Dislocations are included for the basal detachment, the east and southwest rift zones, and the summit region. The geometry of the basal detachment dislocation was constrained by inverting for the fault plane geometry using a uniform slip dislocation prior to applying a non-uniform slip model. The basal detachment dislocation is about 9 km deep at the rift zone, dips 3° to the northwest, and extends 50 km seaward from the rift zone. In the variable-slip inversion, the basal detachment slips a maximum of 17 m and the total moment release is equivalent to a M_w 7.8 earthquake.

Comparison of ground and model displacements indicates that ground displacements significantly exceed model displacements for coastal geodetic stations (Figures 5c and 5d). Footwall stations (Goat, Goat 2, Pilau-3, Panau) remain stationary relative to HVO162, while Apua Pt2, Kaena Pt, and Laeapuki displace horizontally to the southeast 0.8 to 3.4 m. Horizontal and vertical model displacements for coastal geodetic stations are greatest in the west and decrease for eastern stations. The variable-slip dislocation model predicts uplift at the Laeapuki geodetic station. Horizontal ground displacements (solid arrows) exceed horizontal model displacement (open arrows) by as much as ~1.5 m. Vertical ground displacements indicating subsidence also exceed model displacements by up to ~1.5 m.

In order to compare fault offsets across the central Hilina fault system with ground and model displacements, we identify traverses located near three geodetic baselines. Fault offset traverses (Figure 3) are summed along the GOAT-APUA and H162-KAEN baselines to calculate horizontal and vertical fault offsets across the central Hilina fault system (Figures 5e and 5f). No Mauna Ulu lava flows exist near the PANU-LAEP baseline so no fault offset can be calculated. Solid black arrows represent fault

offset across the Hilina faults and solid gray arrows are the residual vectors determined by subtracting the model displacements from ground displacements (i.e., the difference between solid and open arrows in Figures 5c and 5d). Horizontal residual vectors show a transition from southeast to east azimuths for stations farther to the east. The H162-KAEN and PANU-LAEP vertical residual vectors are 18 cm and 16 cm respectively (Figure 5f). For both horizontal and vertical fault offset measurements, the fault offset "overcompensates" the difference between the ground and model displacements by as much as ~1 m. We explain these results in terms of slip on a shallow central Hilina fault system in addition to slip along the deep basal detachment for the Kalapana earthquake.

Discussion of Proposed Model

We begin this discussion by interpreting our ground and model displacements in terms of shallow slip on the central Hilina fault system and deep slip on the basal detachment. Then we present additional support for our shallow fault model interpretation of horizontal block rotation of hanging wall blocks: (1) surface offsets from baseline traverses, (2) line leveling of coseismic elevation changes along the Chain of Craters Road, and (3) plunge of slip vectors on Hilina faults. Finally we discuss the implications of shallow faulting and propose additional research to evaluate the geometry and kinematics of the central Hilina fault system.

Displacement of coastal geodetic stations for the Kalapana earthquake cannot be explained by model displacements from basal detachment slip alone. Horizontal and vertical ground displacements exceed model displacements by as much as ~1.5 m at the surface (Figures 5c and 5d). We suggest that the difference between ground and model displacements represents the amount of secondary slip that occurred on shallow normal faults in the central Hilina fault system. For primary slip on the basal detachment, the

maximum predicted slip is ~17 m at ~9 km depth. Greater amounts of predicted slip on the basal detachment will not explain the large magnitudes and variations of ground displacement; additional shallow faulting is one mechanism that can explain the ground displacements for the Kalapana earthquake. Thus, approximately ten times more slip probably occurred on the basal detachment than on the proposed shallow normal faults for the Kalapana earthquake.

Fault traverses across the central Hilina fault system show that fault offsets are up to ~1 m greater than residual displacements for both horizontal and vertical components (Figures 5e and 5f). In other words, measured extension and downward faulting across the Hilina faults exceed what would be required to match the discrepancy between ground and model displacements for the motions of coastal geodetic stations. Fault offsets from our two baselines have distinct values since each baseline crosses several fault segments at different locations along the fault trace. The southeast-trending residual vector for the H162-KAEN baseline results from the deficiencies in our model inversion to account for the Hilina fault system. Horizontal rotation of hanging wall blocks on shallow-seated faults could produce greater fault offset compared to ground displacements for long baselines across the central Hilina fault system (Figures 2c and 2d). Ground displacements determined from baselines that cross multiple faults indicate a regional displacement whereas fault traverses across several fault scarps document fault offset due to local fault geometry. For example in Figure 2d, the horizontal magnitude of ground displacement and fault offset are probably similar. However, only the fault offset measurements detect the vertical fault offset associated with hanging wall rotation of the two faults. Collapse of the rollover portion of the hanging wall block could produce additional horizontal fault offset

needed to account for the difference between horizontal fault offsets and residual displacements.

Leveling data from the Kalapana earthquake (Lipman et al., 1985) indicate that subsidence occurred on the Chain of Craters Road in regions south of where the road crosses the Holei Pali and Apua Pali faults (Figures 6a and 6b). Projected onto the line of section B-B', the leveling data show ~1.2 m of subsidence south of the Holei Pali fault zone and ~0.75 m of subsidence in the Apua Pali fault zone relative to HVO162. We interpret the leveling data to show horizontal block rotation of hanging wall blocks of the central Hilina fault system rather than localized collapse near the fault zone (Figure 6c). Since no horizontal position measurement is associated with the leveling data, we cannot calculate the horizontal displacement of these leveling stations due to the Kalapana earthquake.

To estimate the subsurface dip of fault surfaces in the Hilina fault system, we determine the plunge of the slip vector for each fault traverse. We utilize the plunge of the slip vector as a proxy for the shallow subsurface dip of the fault surface. The average value for the plunge of slip vectors for all faults in the central Hilina fault system is 20°±17°, suggesting a shallow fault geometry (Figure 6b) rather than a steep fault geometry (Figure 6a). When plunges are grouped by individual fault scarp, values for the plunge of slip vectors on the Poliokeawe Pali, Holei Pali, and Apua Pali faults are 23°±24°, 23°±7°, and 13°±15° respectively (Cannon and Bürgmann, 2001). The plunge of the slip vector at the surface probably represents a maximum fault dip at depth since hanging wall collapse could produce additional vertical fault offset resulting in greater plunges for slip vectors. The azimuths of slip vectors (Figure 3) also suggest a shallow fault geometry. The slip vectors tend to converge along the curved

fault traces of the central Hilina faults suggesting a shallow listric normal fault geometry rather than a deep-seated normal fault geometry.

In using slip vectors to infer subsurface fault dips, we assume that the fault offset observed at the surface is produced by shear slip (mode II fracture) along a subhorizontal detachment (Figure 6d) rather than by extension of a fissure (mode I fracture; Figure 6e). While both scenarios of fault offset are plausible, we prefer the subhorizontal detachment due to the likelihood of subsurface detachment surfaces within the hanging wall blocks. We interpret fault offsets along the GOAT-APUA and H162-KAEN traverses (S_f) to be minimum values of slip at shallow depth (S_s) (Figure 6c). Displacement observed at HVO162 on the footwall of the Hilina fault system results from slip on the basal detachment (S_d) alone. Using slip vectors to make conservative estimates for fault depth, the Holei Pali and Apua Pali faults have fault surfaces that may shallow rapidly to approximately 1 km depth at the coast. However, if the fault surfaces maintain a ~20° dip at depth, the fault surface may be 1-2-km deep at the coast. A few km offshore, these fault surfaces may coincide with a detachment surface at the base of a 2-3-km-thick slump block composed of hyaloclastic material (Morgan et al., 2000). The fault depth may extend down to approximately 5 km, the depth that Riley et al. (1999) calculated for the Puu Kapukapu fault to the west.

Our analysis of ground and model displacements, and fault offsets supports the interpretation of the central Hilina fault system as a series of shallow normal faults. Our work does not refute the idea that the Hilina faults are steeply dipping normal faults but rather provides a mechanism to explain the fault offsets observed for the Kalapana earthquake. Since basal detachment slip in addition to slip on the central Hilina faults displaced the hanging wall blocks, geodetic stations along the coast should

not be included in inversions for basal detachment slip unless the Hilina fault system is explicitly included in the model or accounted for. Otherwise, the inversion of basal detachment slip will be biased by coastal displacements affected by slip on the Hilina fault system. We note, however, that the Hilina faults probably have not slipped during the interseismic periods prior to and following the Kalapana earthquake (Delaney et al., 1998) so removing the coastal stations in basal detachment slip inversions spanning interseismic periods is not necessary.

We hope that future work will focus on refining the three-dimensional structure of the Hilina fault system and resolving the effects of Hilina fault slip on geodetic measurements. The implications of a shallow fault geometry for the Hilina fault system must be considered in future earthquake and tsunami hazard assessment for the Hawaiian Islands. For example, what are the characteristics of an earthquake that could produce a catastrophic submarine landslide originating from the subaerial Hilina fault system? The triggering mechanism of fault slip on a "shallow" rather than "deep" Hilina fault system may be significantly different. Knowledge gained about the stability, structure, and kinematics of the south flank of Kilauea Volcano can be applied to studying and assessing the hazards of other volcanic flanks in the Hawaiian-Emperor volcanic chain and elsewhere around the world.

Conclusions

We compare the 1975 Kalapana earthquake ground displacements derived from analysis of geodetic networks, model displacements calculated from a dislocation model, and fault offsets measured on traverses across the central Hilina fault system to evaluate the potential role of shallow normal faulting as a deformation mechanism for the south flank of Kilauea Volcano, Hawaii. Our existing dislocation model allowing for slip on the basal detachment does not explain motions of geodetic stations along the

coast. Horizontal and vertical ground displacement along the coast are up to ~1.5 m greater than model displacements. Horizontal and vertical fault offset measurements across the central Hilina faults are up to a meter greater than the residual displacement calculated as the difference between the ground and model displacements. We can explain displacements and fault offsets for the Kalapana earthquake if we revise our kinematic model to allow 1) slip on the basal detachment at approximately 9 km depth, and 2) shallow slip and horizontal rotation of hanging wall blocks in the central Hilina fault system.

We interpret the Holei Pali and Apua Pali faults of the central Hilina fault system as shallow normal faults that have a fault dip of about ~20° at the surface. These faults may shallow as they descend, reaching a depth of 1-2 km at the coast, and eventually could intersect the base of a 2-3 km thick hyaloclastic layer (Morgan et al., 2000) offshore. Faults located elsewhere in the Hilina fault system may be more steeply dipping. Continued research is needed to constrain the fault geometry of the Hilina fault system. Accurate structural and kinematic models are fundamental in evaluating the seismic and tsunami hazards associated with the Hilina fault system and the mobile south flank block.

Acknowledgements

This work is supported by U. S. Geological Survey National Earthquake Hazards Reduction Program grant 1434-HQ-98-GR-1024 and a Geological Society of America research grant (E.C.C.). Many thanks to folks at the Hawaiian Volcano Observatory for assistance, especially Michael Lisowski, Asta Miklius, Arnold Okamura, Don Swanson, and Taeko Jane Takahashi We received assistance from Peter Cervelli, Sigurjon Jonsson, and Kristine Larson during fieldwork. James Kellogg and William Chadwick provided fault offset data from their Hilina fieldwork. Juliet Crider, Roger Denlinger,

and Luca Ferrari provided comments to improve this manuscript. We thank our field assistants Jason Bariel, Chad Fleschner, Gwen Pikkarainen, and Jim Weigel for their excellent efforts. Many figures were produced using the Generic Mapping Tools (GMT) program (Wessel and Smith, 1995).

References Cited

Árnadóttir, T., P. Segall, and P. Delaney (1991). A fault model for the 1989 Kilauea south flank earthquake from leveling and seismic data, *Geophys. Res. Lett.* **18**, 2217-2220.

Ando, M. (1979). The Hawaii earthquake of November 29, 1975: Low dip angle faulting due to forceful injection of magma, *J. Geophys. Res.* **94**, 7616-7626.

Bryan, C. J. (1992). A possible triggering mechanism for large Hawaiian earthquakes derived from analysis of the 26 June 1989 Kilauea south flank sequence, *Bull. Seism. Soc. Am*. **82**, 2368-2390.

Cannon, E. C. and R. Bürgmann (2001). Prehistoric fault offsets of the Hilina fault system, south flank of Kilauea Volcano, Hawaii, *J. Geophys. Res.* **106**, 4207-4219.

Chadwick Jr., W. W., J. R. Smith Jr., J. G. Moore, D. A. Clague, M. O. Garcia, and C. G. Fox (1993). Bathymetry of south flank of Kilauea Volcano, *U.S. Geol. Surv. Misc. Field Studies*, map MF-2231.

Delaney, P. T. and R. P. Denlinger (1999). Stabilization of volcanic flanks by dike intrusion, an example from Kilauea, *Bull. Volcan*. (in press).

Delaney, P. T., R. Denlinger, M. Lisowski, A. Miklius, P. Okubo, A. Okamura, and M. K. Sako (1998). Volcanic spreading at Kilauea, 1976-1996, *J. Geophys. Res.* **103**, 18003-18023.

Denlinger, R. P. and P. Okubo (1995). Structure of the mobile south flank of Kilauea Volcano, Hawaii, *J. Geophys. Res.* **100**, 24499-24507.

Dieterich, J. H. (1988). Growth and persistence of Hawaiian volcanic rift zones, *J. Geophys. Res*. **93**, 4258-4270.

Furumoto, A. S., and R. L. Kovach (1979). The Kalapana earthquake of November 28, 1975: An intra-plate earthquake and its relation to geothermal processes, *Phys. Ear. Plan. Int.* **18**, 197-208.

Gillard, D., M. Wyss, and P. Okubo (1996). Type of faulting and orientation of stress and strain as a function of space and time in Kilauea's south flank, Hawaii, *J. Geophys. Res.* **101**, 16025-16042.

Got, J.-L., F. W. Fréchet, and W. Klein (1994). Deep fault plane geometry inferred from multiplet relative relocation beneath the south flank of Kilauea, *J. Geophys. Res.* **99**, 15375-15386.

Hill, D. P. (1969). Crustal structure of the island of Hawaii from seismic-refraction measurements, *Bull. Seism. Soc. Am.* **59**, 101-130.

Hill, D. P. and J. J. Zucca (1987). Geophysical constraints on the structure of Kilauea and Mauna Loa volcanoes and some implications for seismomagmatic processes, in *Volcanism in Hawaii,* R. W. Decker, T. L. Wright and P. H. Stauffer (Editors), *U. S. Geol. Surv. Prof. Pap.* **1350**, 903-917.

Jackson, M. D., E. T. Endo, P. T. Delaney, T. Árnadóttir, and A. M. Rubin (1992). Ground Ruptures of the 1974 and 1983 Kaoiki Earthquakes, Mauna Loa Volcano, Hawaii, *J. Geophys. Res.* **97**, 8775-8796.

Kellogg, J. N. and W. Chadwick (1987). Neotectonic study of the Hilina fault system, Kilauea, Hawaii (abstract), *Geol. Soc. Am. Abstracts with Programs* **19**, 394.

Lipman, P. W., J. P. Lockwood, R .T. Okamura, D. A. Swanson, and K. M. Yamashita (1985). Ground deformation associated with the 1975 magnitude-7.2 earthquake and resulting changes in activity of Kilauea Volcano, Hawaii, *U. S. Geol. Surv. Prof. Pap.* **1276**.

Ma, K.-F., H. Kanamori, and K. Satake (1999). Mechanism of the 1975 Kalapana, Hawaii, earthquake inferred from tsunami data, *J. Geophys. Res.* **104**, 13153-13167.

Matthews, M. V. and P. Segall (1993). Estimation of depth-dependent fault slip from measured surface deformation with application to the 1906 San Francisco earthquake, *J. Geophys. Res.* **98**, 12153-12163.

Moore, J. G. and R. S. Fiske (1969). Volcanic substructure inferred from dredge samples and ocean-bottom photographs, Hawaii, *Geol. Soc. America Bull.* **80**, 1191-1202.

Moore, J. G., W. R. Normark, and R. T. Holcomb (1994). Giant Hawaiian underwater landslides, *Science* **264**, 46-47.

Moore, J. G. and W. W. Chadwick (1995). Offshore geology of Mauna Loa and adjacent areas, Hawaii, in *Mauna Loa Revealed,* J. M. Rhodes and J. P. Lockwood (Editors), *AGU Geophys. Monograph* **92**, 21-44.

Morgan, J. K., G. F. Moore, D. J. Hill, and S. Leslie (2000). Overthrusting and sediment accretion along Kilauea's mobile south flank, Hawaii: Evidence for volcanic spreading from marine seismic reflection data, *Geology* **28**, 667-670.

Nakamura, K. (1980). Why do long rift zones develop better in Hawaiian volcanoes? A possible role of thick ocean sediment, *Bull. Volcano. Soc. Japan* **25**, 255-269.

Okubo, P. G., H. M. Benz, and B. A. Chouet (1997). Imaging the crustal magma sources beneath Mauna Loa and Kilauea volcanoes, Hawaii, *Geology* **25**, 867-870.

Okubo, P. G. and J.-L. Got (1999). Constraints on fault geometry based on precise relative relocations of Hawaiian seismicity (abstract), *Eos Trans. AGU*, **80**, 666.

Owen, S., P. Segall, J. Freymueller, A. Miklius, R. Denlinger, T. Árnadóttir, M. Sako, and R. Bürgmann (1995). Rapid deformation of the south flank of Kilauea Volcano, Hawaii, *Science* **267**, 1328-1332.

Owen, S., P. Segall, M. Lisowski, A. Miklius, R. Denlinger, J. Freymueller, T. Árnadóttir, T., and M. Sako (2000). The rapid deformation of Kilauea Volcano: GPS measurements between 1990 and 1996, *J. Geophys. Res.* **105**, 18983-18998.

Riley, C. M., J. F. Diehl, J. L. Kirschvink, and R. L. Ripperdan (1999). Paleomagnetic constraints on fault motion in the Hilina Fault System, south flank of Kilauea Volcano, Hawaii, *J. Volcano. Geotherm. Res.* **94**, 233-249.

Rubin, A. M., D. Gillard, and J.-L. Got (1999). Streaks of microearthquakes along creeping faults, *Nature* **400**, 635-641.

Swanson, D. A., W. A. Duffield, and R. S. Fiske (1974). Displacement of the south flank of Kilauea Volcano: The result of forceful intrusion of magma into the rift zones, *U. S. Geol. Surv. Prof. Pap.* **963**.

Thurber, C. H. and A. E. Gripp (1988). Flexure and seismicity beneath the south flank of Kilauea Volcano and tectonic implications, *J. Geophys. Res*. **93**, 4271-4278.

Tilling, R. I.., R. Y. Koyanagi, P. W. Lipman, J. P. Lockwood, J. G. Moore, and D. A. Swanson (1976). Earthquake and related catastrophic events Island of Hawaii, November 29, 1975: A preliminary report, *U. S. Geol. Surv. Circular* **C 0740**.

Wessel, P. and W. H. F. Smith (1995). New version of the Generic Mapping Tools released, *EOS Trans. AGU* **76**, 329.

Wyss, M. (1988). A proposed source model for the Great Kau, Hawaii, earthquake of 1868, *Bull. Seismo. Soc. Am.* **78**, 1450-1462.

Figures

Figure 1. Location map of south flank of Kilauea Volcano. Faults of Hilina fault system include Hilina Pali, Puu Kapukapu, Poliokeawe Pali, Holei Pali, and Apua Pali. Star indicates 1975 Kalapana earthquake epicenter. Solid vectors represent horizontal displacement (2-sigma error ellipses) for 1975 Kalapana earthquake calculated from model coordinate solution of available 1974-1976 trilateration data corrected for displacements in a large December 1974 Southwest rift zone intrusion. Scale vector represents 5 m horizontal displacement. Stations identified with * are not included in the model inversion. Line of section A-A' in Figure 2.

Figure 2. (a) Northwest-southeast cross-section A-A' of south flank of Kilauea Volcano. Cross-section has no vertical exaggeration. Dots show microseismicity from Gillard et al. (1996); ocean plate geometry from Hill and Zucca (1987). Pelagic sediment layer and thrust faults (dotted lines) interpreted from marine seismic profiles (Morgan et al., 2000). Hilina fault system depicted as either deep normal fault (long-dash line – 75° dip from Okubo et al., 1997) or shallow normal faults (short-dash, curved lines). (b) to (d) Block diagrams of possible fault geometry for Hilina fault system. For each diagram, a slip triangle indicates the amount of total slip (s) with horizontal (h) and vertical (v) slip components. (b) steep 60° dipping normal fault; (c) shallow 30° dipping normal fault and horizontal detachment; (d) two shallow 30° dipping normal faults on horizontal detachments. (c) and (d) are area-balanced with geodetic stations shown with solid triangles. Note difference between ground displacement and fault offset in (d).

Figure 3. Map of (a) horizontal and (b) vertical fault offsets for Kalapana earthquake; error bounds represent summed measurement error of individual piercing points; scale vector is 1 m fault offset. For both maps: solid vectors indicate new data

(data presented in Table DSM_1); open vectors indicate data from Kellogg and Chadwick (1987); 1969-1974 Mauna Ulu flows shaded gray; older lava flows shown in white; dashed lines bound the location of fault scarps; Chain of Craters Road indicated with bold line. Inset in (a) shows an example of individual fault offsets contributing to an overall fault offset across a fault scarp. Individual horizontal fault offsets "a" to "r" are summed to produce horizontal fault offset vector T50. South-trending vectors in (b) represent hanging wall-down fault offset.

Figure 4. Schematic diagram of contributions of shallow normal faulting and basal detachment slip to observed fault offsets. Triangles represent geodetic stations; solid vectors are ground displacements; open vectors indicate predicted model displacements from a coseismic dislocation model of detachment slip computed from data excluding coastal sites. Residual displacements (s1 and s2) determined from difference between ground displacement and model displacement are partly attributable to shallow normal faulting. The baseline (BL) vector represents fault offset at surface calculated from traverses across fault scarps. Thick black lines at top of fault scarps indicate regions of surface fractures observed in the field.

Figure 5. Ground displacements, model displacements, and observed fault offsets for Kalapana earthquake. Figures (a), (c), and (e) use arrows to indicate horizontal displacements and fault offsets. Figures (b), (d), and (f) use north-south oriented arrows with flattened heads to indicate vertical uplift (north-oriented arrow) and subsidence (south-oriented arrow). (a) and (b) Ground displacements calculated relative to HVO162 (Tilling et al., 1976; Lipman et al, 1985). (a) Horizontal ground displacements computed in a model coordinate solution of coseismic line-length changes using EDM (Electronic Distance Measurements) and (b) vertical ground displacements from tide gage and leveling measurements. Location of HVO 162 and

outline for (c) to (f) shown. (c) to (f) Geodetic station HVO162 indicated with solid triangle. (c) and (d) Ground displacements (solid vectors) and model slip on basal detachment (open vectors) for horizontal (c) and vertical (d) motions (2-sigma error bounds). (e) and (f) Integrated horizontal (e) and vertical (f) fault offsets across baselines. Solid black vectors (labeled "BL") represent summed surface fault offsets along baselines (error bounds from estimated measurement error); solid gray vectors indicate residual displacements calculated from difference between ground and model displacements in (c) and (d) (2-sigma error ellipses).

Figure 6. (a) Location map of leveling stations (solid dots) along Chain of Craters (CoC) Road (dashed line). Fault scarps shaded gray. Line of section B-B' indicated on map. (b) Leveling data from 1975 Kalapana earthquake (Lipman et al., 1985) calculated relative to HVO162 and projected onto line of section B-B'. (c) Schematic diagram showing possible hanging wall geometry of shallow Hilina fault system along line of section B-B'. Cross-section has no vertical exaggeration; dashed lines represent possible fault subsurface fault geometry for Holei and Apua Pali faults. Dotted lines represent possible dip of lava flows from hanging wall rotation based on paleomagnetic estimates near Puu Kapukapu (Riley et al., 1999). Slip vector abbreviations are: s_f, slip vector at surface calculated from fault offset traverses; s_s, slip vector on shallow detachment; s_d, slip vector on deep detachment. (d) and (e) Schematic diagrams of surface fracture resulting from (d) shear slip of a mode II fracture on a subhorizontal detachment and (e) fissuring due to extension of a mode I fracture.

Table 1
Kalapana Earthquake Fracture Characteristics for Hilina Faults

Hilina Fault	Average Fracture Trend* (°)	Average Piercing Point Azimuth* (°)	Horizontal Offset Average[§] (m) ± σ	Horizontal Offset Maximum[#] (m) ± σ	Vertical Offset Average[§] (m) ± σ	Vertical Offset Maximum[#] (m) ± σ
Poliokeawe Pali	088±002; n=522	180±008; n=52	1.27±0.64	1.95±0.05	-0.16±0.21	-0.53±0.03
Holei Pali	074±003; n=192	151±005; n=26	1.09±0.85	2.80±0.23	-0.50±0.51	-1.71±0.02
Apua Pali	068±002; n=691	155±004; n=186	0.35±0.23	0.82±0.02	-0.06±0.13	-0.43±0.04

Uncertainties are given as: *95% confidence (2-σ) of n measurements; §standard deviation of horizontal or vertical displacements (1-σ); #instrument measurement uncertainty (1-σ) for traverse with maximum fault offset.

Digital Supplemental Material: Average Fracture Trend data presented in Table DSM_2; Average Piercing Point Azimuth data presented in Table DSM_3.

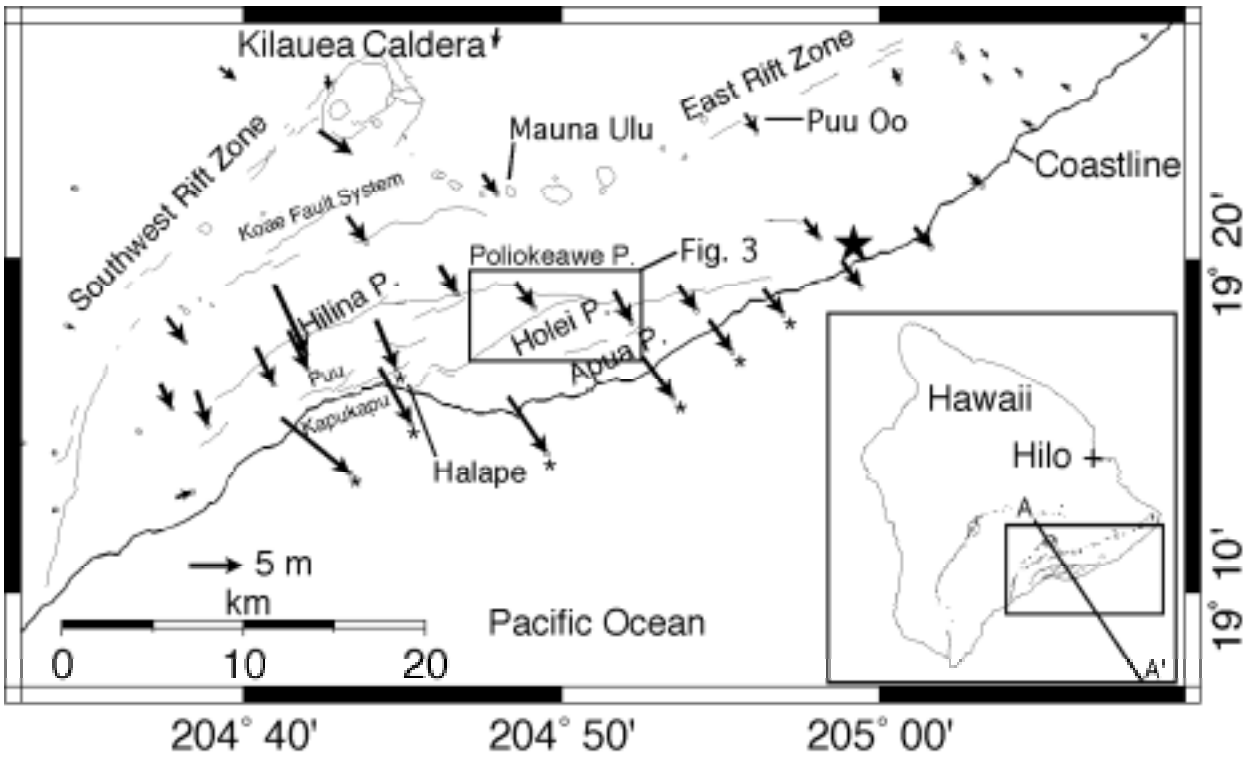
Kilauea Caldera
Southwest Rift Zone
East Rift Zone
Mauna Ulu
Puu Oo
Coastline
Koae Fault System
Poliokeawe P.
Fig. 3
Hillina P.
Holei P.
Apua P.
Puu Kapukapu
Halape
Hawaii
Hilo
A
A'
5 m
km
0
10
20
Pacific Ocean
19° 20'
19° 10'
204° 40'
204° 50'
205° 00'

Figure 1

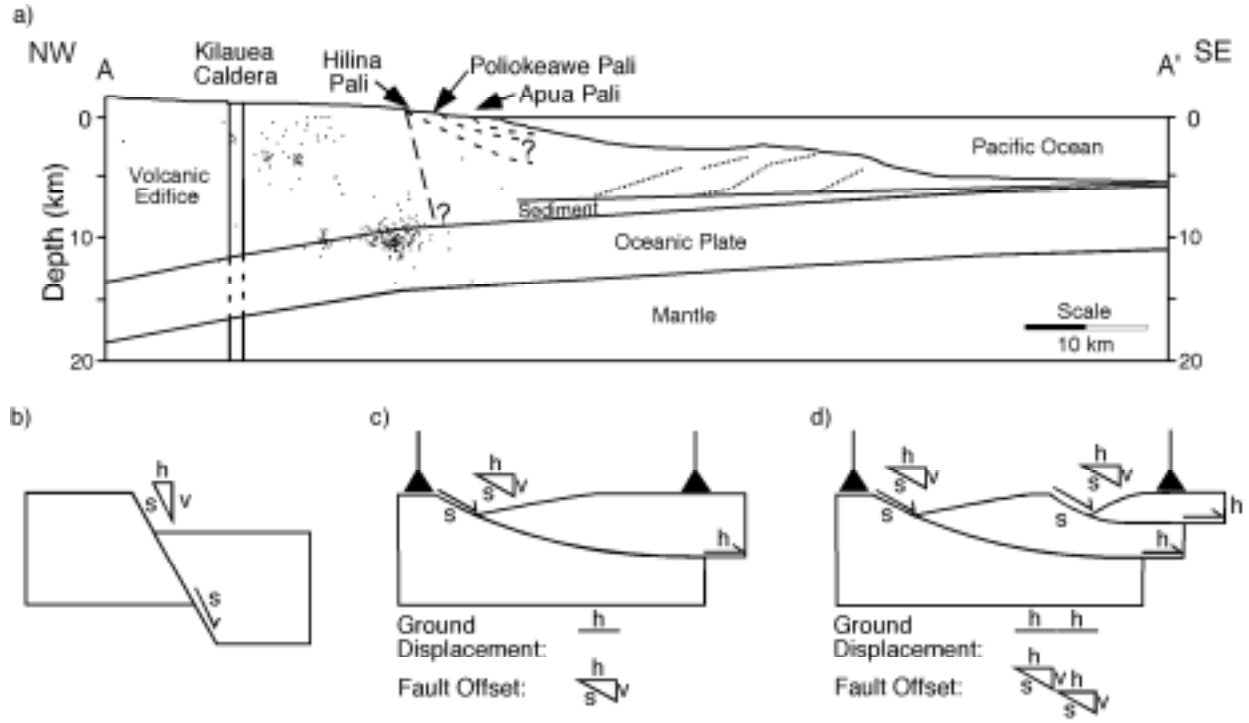
a)
NW
A
Kilauea Caldera
Hilina Pali
Poliokeawe Pali
Apua Pali
A'
SE
Depth (km)
Volcanic Edifice
Pacific Ocean
Sediment
Oceanic Plate
Mantle
Scale
10 km
b)
c)
d)
Ground Displacement:
Fault Offset:
Ground Displacement:
Fault Offset:

Figure 2

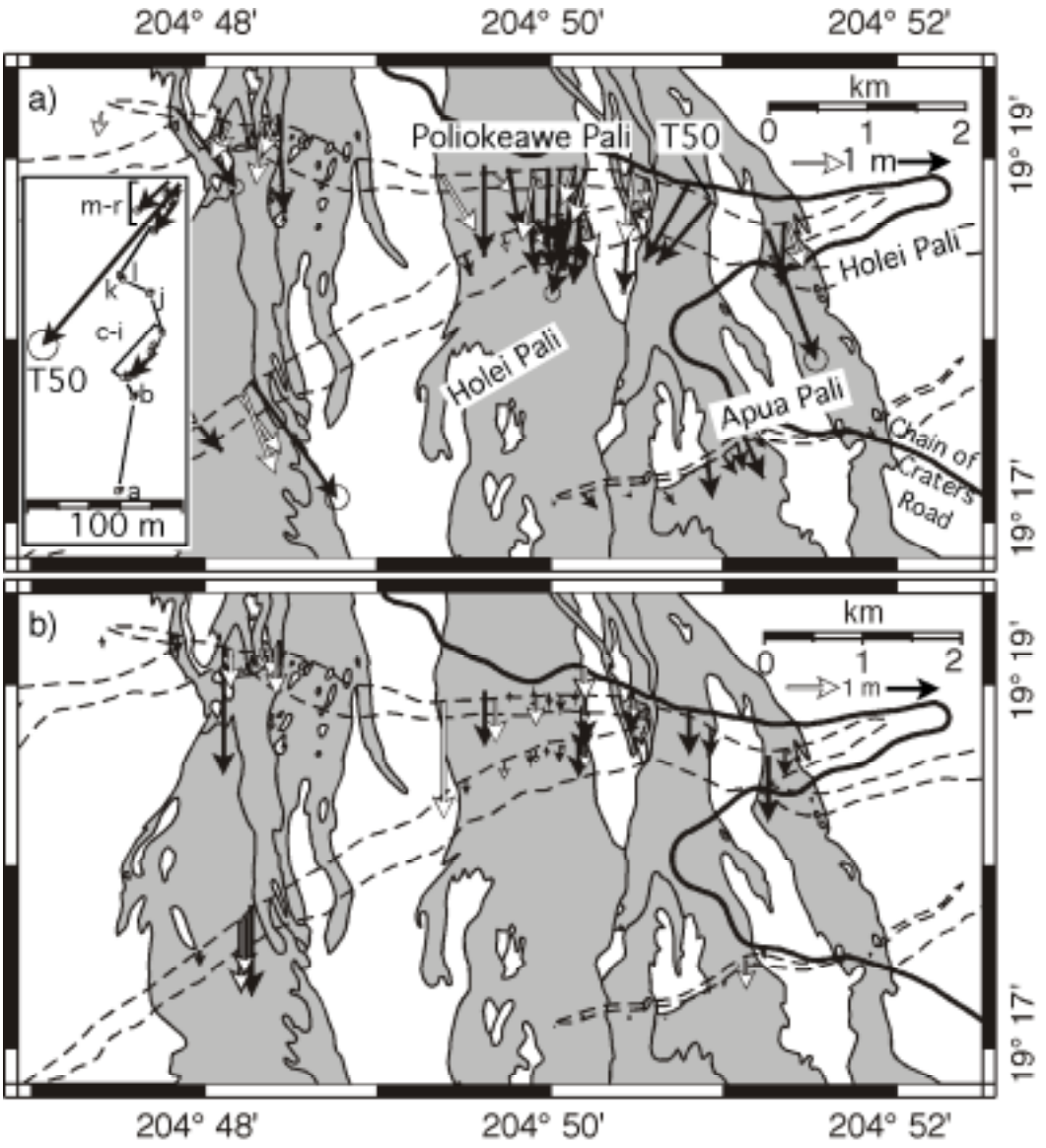
204° 48'
204° 50'
204° 52'
a)
km
0 1 2
1 m
Poliokeawe Pali
T50
Holei Pali
Holei Pali
Apua Pali
Chain of Craters Road
m-r
k
l
j
c-i
T50
b
a
100 m
19° 19'
19° 17'
b)
km
0 1 2
1 m
19° 19'
19° 17'
204° 48'
204° 50'
204° 52'

Figure 3

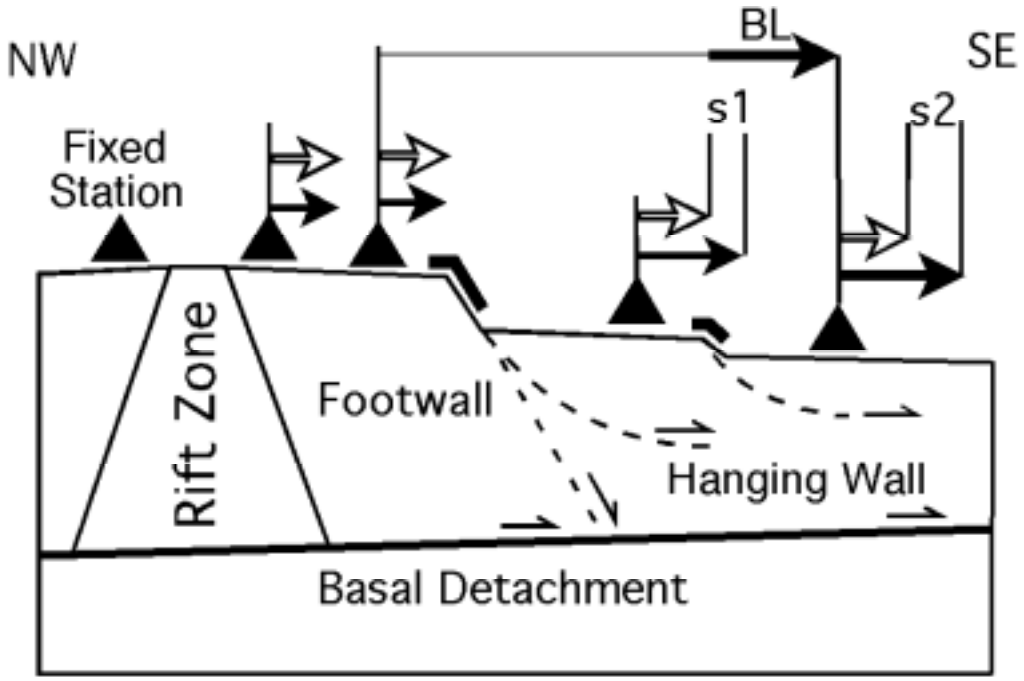
NW
BL
SE
s1
s2
Fixed
Station
Rift Zone
Footwall
Hanging Wall
Basal Detachment

Figure 4

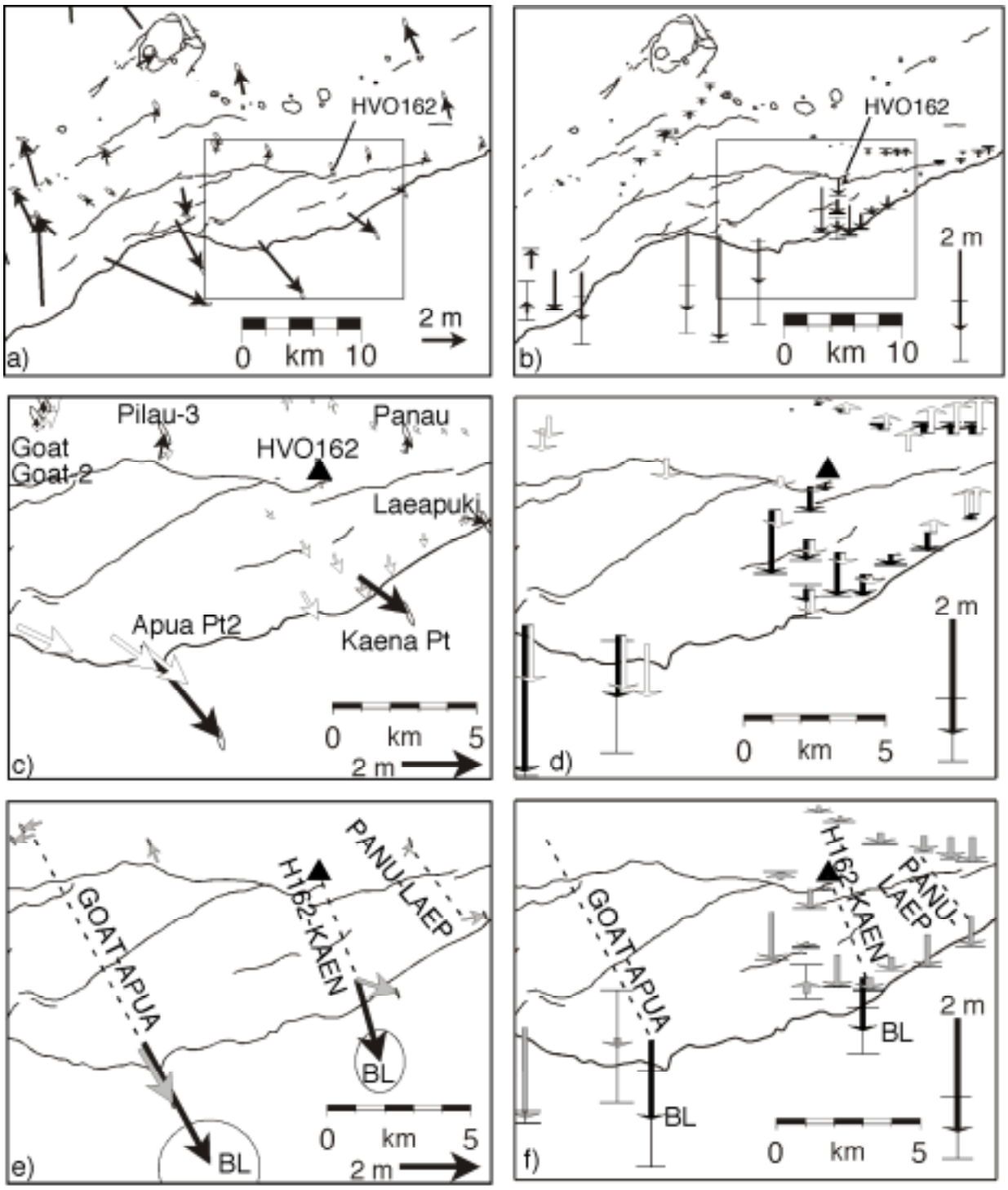
HVO162
2 m
0 km 10
a)
HVO162
2 m
0 km 10
b)
Pilau-3
Panau
Goat
Goat-2
HVO162
Laeapuki
Apua Pt2
Kaena Pt
0 km 5
2 m
c)
2 m
0 km 5
d)
PANU-LAEP
H162-KAEN
GOAT-APUA
BL
0 km 5
2 m
e)
H162-KAEN
PANU-LAEP
GOAT-APUA
BL
BL
2 m
0 km 5
f)

Figure 5

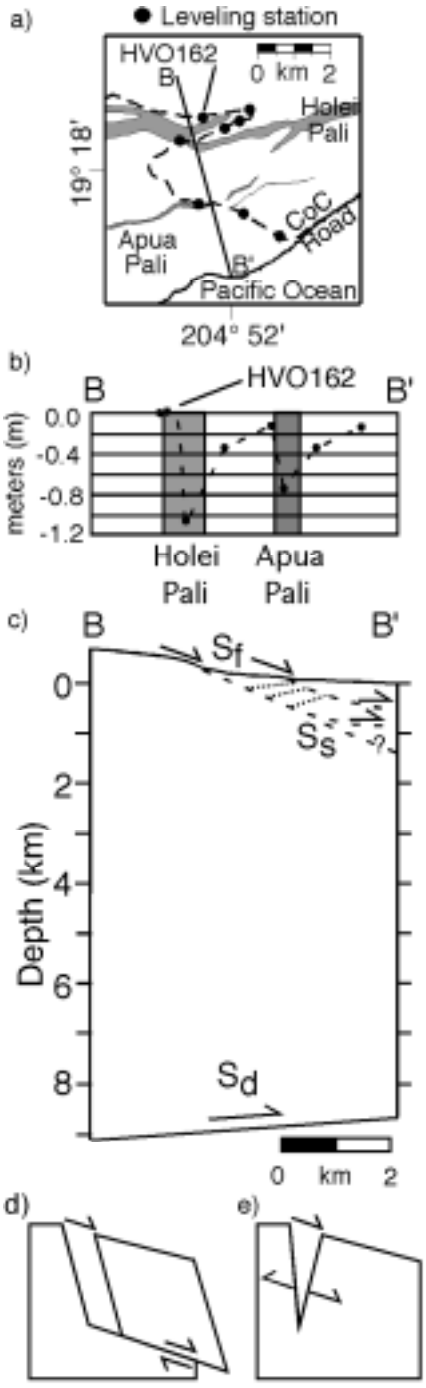
a)
Leveling station
HVO162
B
0 km 2
Holei Pali
19° 18'
CoC Road
Apua Pali
B'
Pacific Ocean
204° 52'
b)
B
HVO162
B'
meters (m)
0.0
-0.4
-0.8
-1.2
Holei Pali
Apua Pali
c)
B
B'
Sf
Ss
Depth (km)
0
2
4
6
8
Sd
0 km 2
d)
e)

Figure 6